Journal of Alloys and Compounds 720 (2017) 221–229

Contents lists available at ScienceDirect

Journal of Alloys and Compounds

journal homepage: http://www.elsevier.com/locate/jalcom

Effective removal of metal ions from aqueous solution by mesoporous MnO_2 and TiO_2 monoliths: Kinetic and equilibrium modelling

Manisha Sharma [a], Diptiman Choudhury [a], Satyajit Hazra [b], Soumen Basu [a, *]

[a] School of Chemistry and Biochemistry, Thapar University, Patiala 147004, India
[b] Saha Institute of Nuclear Physics, Kolkata 700064, India

ARTICLE INFO

Article history:
Received 10 March 2017
Received in revised form
10 May 2017
Accepted 25 May 2017
Available online 26 May 2017

Keywords:
Nanocasting
Mesoporous
Monoliths
Metal-oxide
Metal-ions adsorption
Wastewater treatment

ABSTRACT

In the present study, ordered hierarchically porous silica (by sol-gel method) and metal-oxide monoliths (through nanocasting method) were synthesized. Porous silica and metal oxide monoliths (MnO_2 and TiO_2) exhibited excellent adsorption for heavy metal ions such as Pb(II) & Cd(II). The morphological and structural study of the synthesized silica and metal oxide monoliths were done by FESEM and XRD analysis. The adsorption studies were conducted in different batches. The maximum adsorption of Pb(II) on SiO_2, MnO_2 and TiO_2 varied from 91 to 125, 166–200 and 769–857 mg/g respectively depending upon the choice of PEG, which is used as a structure directing/controlling agent. Similarly the maximum adsorption of Cd(II) on SiO_2, MnO_2 and TiO_2 varied from 90 to 100, 100–125 and 667–770 mg/g respectively. The effects of contact time (0–80 min), temperature (at 303, 313 and 323 K) and pH (3–10) on the Pb(II) & Cd(II) removal were also explored.

1. Introduction

Removal of heavy metals from wastewater is very important to reduce the environmental toxicant load. Heavy metals are non-biodegradable and cause serious consequences when present in aquatic and soil ecological system. The pollutant in water hinders aquatic life [1] and bioaccumulation of pollutants in the ecosystem and their potential health risks are of great concern [2] such as multiple organ damages, change in cell cycle and may cause carcinogenic diseases [3,4]. From the economic, environmental, human, animal and microbial health perspective, removal of heavy metals from water is mandatory. Heavy metal's leaching is an important issue. From various sources including chemical industrial waste such as printing waste, battery waste, paper manufacturing, chemical manufacturing, food, pharmaceutical, textile [5], smelting, commercial fertilizer, pesticides, sewage sludge, metal evaporation from water resource to soil and groundwater [6,7], water get polluted with heavy metals.

Among the various heavy metal ions, lead and cadmium have been accepted as one of the main concern pollutants [8]. Porous materials are very effective for removal of these toxicants. At present, most of the available adsorbents are specific for a particular type of metal ion and hence can be useful for removal of only that one. Since water get polluted by different heavy metal contaminants; it would be useful to synthesize a single nanomaterial that can absorb/trap different types of heavy metal ions. Various metal oxides such as MgO, CuO, Fe_2O_3, ZnO, TiO_2 and MnO_2; can be utilized to make useful mesoporous nanomaterials [9]. These metal oxides are non-toxic and less expensive and therefore very useful to purify large water bodies.

Porous metal-oxides (MnO_2 and TiO_2) are very attractive for this purpose because of their surface active properties [10–12]. Also, MnO_2 and TiO_2 shows promising catalytic properties and remarkable potential for waste water treatment to remove a wide range of metal-ions (e.g. lead and cadmium) [13,14]. In literature, it is found that MnO_2-coated MWCNTs were used for removal of Pb(II) from water using packed column and removal was measured up to 95% [15]. Zaman et al. in 2009 investigated the effect of phosphate complexation on Cd(II) adsorption by β-MnO_2 and maximum adsorption efficiency measured was 3.515×10^{-5} mol/g [16]. The MnO_2-loaded resin had been used as an adsorbent for lead and cadmium removal and the maximum removal efficiency was calculated as 80.64 mg/g for Pb(II) and 21.45 mg/g for Cd(II) [17]. Some research had been done on the removal of Cd^{2+}, Cu^{2+}, Ni^{2+}, and Pb^{2+} from synthetic solutions using nanoparticle sorbents (TiO_2, MgO, and Al_2O_3) with a range of experimental approaches

* Corresponding author.
E-mail address: soumen.basu@thapar.edu (S. Basu).

http://dx.doi.org/10.1016/j.jallcom.2017.05.260
0925-8388/

[9]. Flower-like TiO_2-graphene oxide was used for the removal of heavy metal ions from water. The removal capacity of TiO_2-graphene oxide was measured 88.9, 72.8 and 65.6 mg/g for Zn^{2+}, Cd^{2+}, and Pb^{2+}, respectively [18]. The adsorption of Pb (II), Cu (II) and Zn (II) by TiO_2 can be accomplished from simulated polluted water and up to 94% removal was achieved [19]. The titania beads were used to remove Cr(VI), Cd(II), Cr(III), Cu(II), and Co(II) ions from simulated wastewater and the adsorption capacities were found to be 9.39, 8.94, 8.93, 8.40, and 7.62 mg g^{-1}, respectively [20]. So from these studies, it is obvious that there is a huge demand to synthesize hierarchically porous MnO_2 and TiO_2 materials with the tunable high surface area and high selective adsorption efficiency. In spite of huge demand, most of the available materials are not user-friendly and eco-friendly. Mostly metal-oxide nanomaterials are available in powder form which has disadvantages since they make a miscible suspension with water. Therefore; for their extraction from solution, expensive high-quality filters, and instruments are necessary. So in this regard, we tried to make hierarchically porous MnO_2 and TiO_2 metal-oxide monoliths (single rock like structure) for metal-ion adsorption which is cost-effective and user-friendly. The efficient removal of metal-ions using solid monoliths synthesized by nanocasting method has not been studied yet.

Metal-oxide monoliths with hierarchically porous structures can be prepared by using nanocasting process. In this method at first pores of the parental silica monoliths have been saturated with a choice of metal salt solution. Thereafter by heat treatments, the metal salt is converted to corresponding metal oxides. At the end, silica part gets removed by either KOH or NaOH [21]. This process has already been used to prepare porous nanomaterials and monoliths of carbon, NiO, TiO_2, Co_3O_4, SnO_2, MnO_2, ZrO_2, Cr_2O_3, In_2O_3, CeO_2, Fe_2O_3, Y_2O_3 and various or mixed-oxides [22–30]. Ordered porous oxides because of their large surface areas, large pore volumes and ordered pore networks have a wide range of potential applications in energy storage, nanoreactors, semiconductors, electronic devices, catalysis and gas sensors [31]. The application of these metal oxide monoliths is highly dependent on their pore diameter as well as their surface properties. By altering the pore diameter of the parental monolith, it is possible to change the porous structure of progeny metal oxide monoliths. The formation of meso/micropores is highly dependent on the nature and concentration of structure directing agents (e.g. surfactants/water soluble polymers).

As the metal oxide monoliths are the inverse replicas of parental monoliths, so it is possible to control the porosity of the replica monolith by changing the porosity of parent silica monoliths. By exploring this fact, we have synthesized various pore size controlled TiO_2 and MnO_2 monoliths by a nanocasting method using parent mesoporous silica monoliths. To explore the effect of pore diameter/surface area on the application of metal oxide monoliths, we have thoroughly studied the adsorption efficiency of these metal-oxide monoliths for the removal of metal ions such as Pb(II) & Cd(II). The effects of contact time, temperature, pH and adsorbent concentration for removal of metal ions were also explored. The kinetic and equilibrium studies of the monoliths were done by Langmuir and Freundlich Isotherms.

2. Material and methods

2.1. Materials

Manganese nitrate and Tetraethoxysilane (TEOS) were purchased from Alfa Aesar, England. Polyethylene glycol (PEG) (MW 4000 & 35,000 g/mol) and Cetyltrimethyl bromide (C_{18}TAB) were purchased from Sigma-Aldrich, USA. Lead nitrate, cadmium carbonate and titanium tetrachloride were obtained from Spectrochem, India. Nitric acid (69%) and Ammonia (28–30%) were purchased from Merck, India. All the reagents were of analytical grade. All reagents were used without further purification. All synthetic solutions of metal ions were prepared with milli-Q water.

2.2. Characterization of monoliths

X-ray diffraction analysis (XRD) was performed using PANALYTICAL X'Pert PRO X-ray diffractometer having Cu Kα (λ = 1.540 Å) radiation operated at 45 KV. For field emission scanning electron microscopy (FESEM), JEOL- 7000 FESEM equipped with Energy Dispersive X-ray Spectroscopy (EDX) detector was used. Surface area was analyzed through BET surface area analyzer of Microtrac BEL Corp. Pvt. Ltd, Japan (Microtec Belsorp Mini–II). Atomic adsorption spectrophotometer (AAS) of GBC 932AA was used to analyze the metal ion concentrations.

2.3. Experimental procedures

2.3.1. Synthesis of silica monoliths

TEOS (8.1 ml) was added to a mixture of PEG (9.54 × 10-4 M) and 1.38 ml nitric acid (30%) solution in 8.25 ml distilled water and then mixed by stirring at room temperature for 5–10 min until a translucent sol was obtained. After that, 1.3 g CTAB was added to the sol with continuous agitation until the surfactant was dissolved completely. Here, CTAB was used as surfactant template for formation of mesoporous structures in monoliths. The obtained sol was transferred to microplates and 8–12 h time was required for sol to gel formation at 40 °C. Thereafter aging of the gel was done at 40 °C for 72 h. To increase the degree of condensation and stability of the SiO_2 monoliths, the solvent exchange was performed. Silica monoliths were soaked in (1M) NH_4OH solution for 9 h at 90 °C. Later, SiO_2 monoliths were acidified by using (0.1 M) HNO_3 solution. After washing with de-ionized water, monoliths were kept in an oven at 40 °C for 4–5 days for proper drying. Finally, freshly prepared monoliths were calcined at 550 °C for 5 h using 1 K/min heating ramp.

2.3.2. Nanocasting

SiO_2 monoliths were degassed using a vacuum pump and then impregnated with aqueous metal salt solutions [3.1 M $Mn(NO_3)_2 \cdot 4H_2O$ and 2.7 M $TiCl_4$] by incipient wetness. After the first cycle of impregnation, monoliths appeared transparent. After that, the monoliths were heated for 10 h at 150 °C and 100 °C for MnO_2 and TiO_2 respectively. These two steps were repeated for 5 times. Afterward, composites of MnO_2 were calcined at 300 °C for 6 h with 1 K/min heating ramp. Finally, silica part was leached out from both of the composites to get metal-oxide monoliths by using NaOH (2 M). Schematic diagram of the synthesis process for parent SiO_2 along with MnO_2 & TiO_2 metal-oxide monoliths is shown in Scheme 1. By changing the chain length of polymer (PEG), it is possible to alter the morphology of the silica monoliths along with the morphology of the metal-oxide monoliths as well. Synthesized monoliths were in the cm range scale (0.5 cm in diameter and 0.8 cm in length). The final MnO_2 monoliths appeared black while the TiO_2 were beige in color.

2.4. Adsorption study

Metal ions adsorption on the metal-oxide monoliths was executed in a batch system at ambient temperature using favorable conditions. Dry silica/metal-oxide monolith (MnO_2 & TiO_2) (0.02 g) was added into a 100 ml of synthetic metal ion solution (10–50 mgL^{-1}) and agitated for different time periods at a speed of

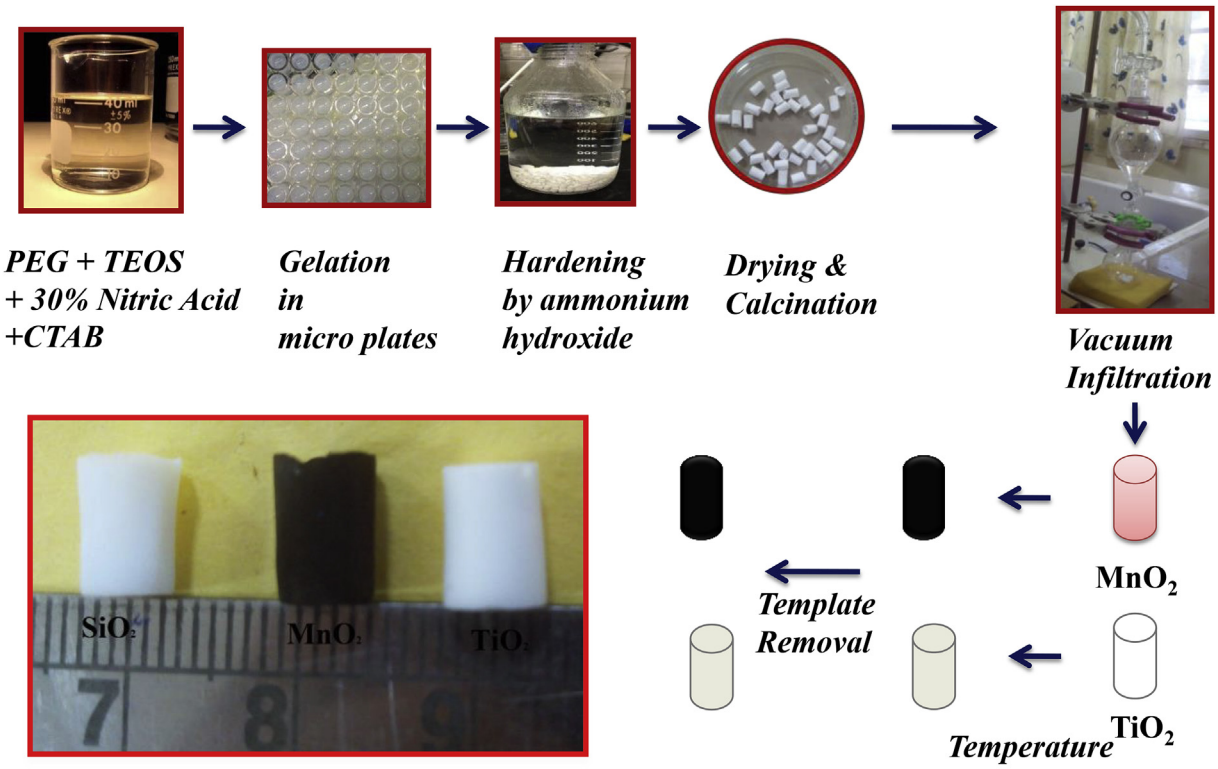

Scheme 1. Schematic representation of synthesis of porous silica monolith and metal-oxide monoliths with different pore size/surface area.

200 rpm. After the adsorption period, the solution was centrifuged for 10 min at 6000 rpm and the supernatant solutions were analyzed to determine the residual metal ion concentration left in the solution by AAS. AAS was used to analyze the dissolved Pb(II) & Cd(II) from a standard solution of lead nitrate and cadmium carbonate respectively, using calibration curve. The adsorption capacity (q_e) was calculated by the uptake amount of metal ions adsorbed per mass unit of monoliths (mg/g) using the formula:

$$q_e = \frac{(C_o - C_e)}{m} \times V \quad (1)$$

where C_o is the initial and C_e is the equilibrium concentration (mg/L), while V is the volume of the solution (L) and M is the weight of the adsorbent (g). To control precision, each one of the adsorption experiments were performed in triplicates and average value was reported.

3. Results and discussion

As mentioned above nanocasting is a simple method for synthesis of porous metal-oxide monoliths. For stabilization of mesoporous silica monoliths, the water soluble polymer is needed because they have a direct effect on hydrophilicity and flexibility of the porous structure. Bimodal interconnected porous structures obtained by phase separation and gelation after interaction (hydrogen bonding) between gelling silica/CTAB micelles and polymer. White gels having bimodal structures can be obtained by addition of polymer with increasing chain length due to a decrease in phase separation time [32,33].

In this regard, PEG with different chain length/molecular weight (4000 and 35,000 g/mol) had been used as the water soluble polymer. In Fig. 1A, the nitrogen sorption isotherms of the SiO_2, MnO_2 & TiO_2 monoliths with a different chain length of PEG are plotted. The surface area and pore volume decreased whereas pore size increased when SiO_2 monoliths were replaced by metal oxide monoliths (Table 1). For all synthesized samples, type IV isotherms could be observed as confirmed from the IUPAC classification. The uniformity of pore sizes and shape were defined by the sharp adsorption and desorption branches in H1 hysteresis loops of the synthesized hierarchically porous silica monoliths. Fig. 1B shows the pore size distribution by using the Barrett–Joyner–Halenda (BJH) method of as synthesized monoliths, which confirms the mesoporosity nature of the monoliths. After the removal of silica part, the crystal phase composition of the metal-oxide monoliths was determined by XRD analysis. Fig. 1C shows the diffraction patterns of metal-oxide monoliths. It was observed that after calcining at 300 °C, monoliths impregnated with manganese nitrate resulted in the formation of β-MnO_2. The diffraction peaks were confirmed by JCPDS card No. 24–0735 [34]. While TiO_2 was obtained from $TiCl_4$ and the peaks for rutile and anatase were confirmed by JCPDS card No. 21–1272 [35].

Mechanically steady metal-oxide monoliths were retrieved by nanocasting method upon the leaching of the silica portion. Influence on the homogeneity of monoliths structure of the SiO_2, MnO_2 and TiO_2 was analyzed using FESEM. Fully interconnected pores were formed by the phase separation in metal-oxides monoliths. The porous structures of the monoliths with different PEG are shown in Fig. 2 (molecular weight 35,000 series) and in Fig. SI 1 (molecular weight 4000 series). There appear to be fine mesoporous structures within the walls, but higher magnification images are difficult to obtain due to the charging of the sample. Metal-oxide monoliths have rough mesoporous walls as compared to silica monoliths. The purity of the metal oxide monoliths (almost complete removal of SiO_2) was confirmed by EDX analysis (Fig. 2 and Fig. SI 1). Uniform distribution of the precursor metal salts throughout the core of the SiO_2 monoliths was responsible for chemical homogeneity.

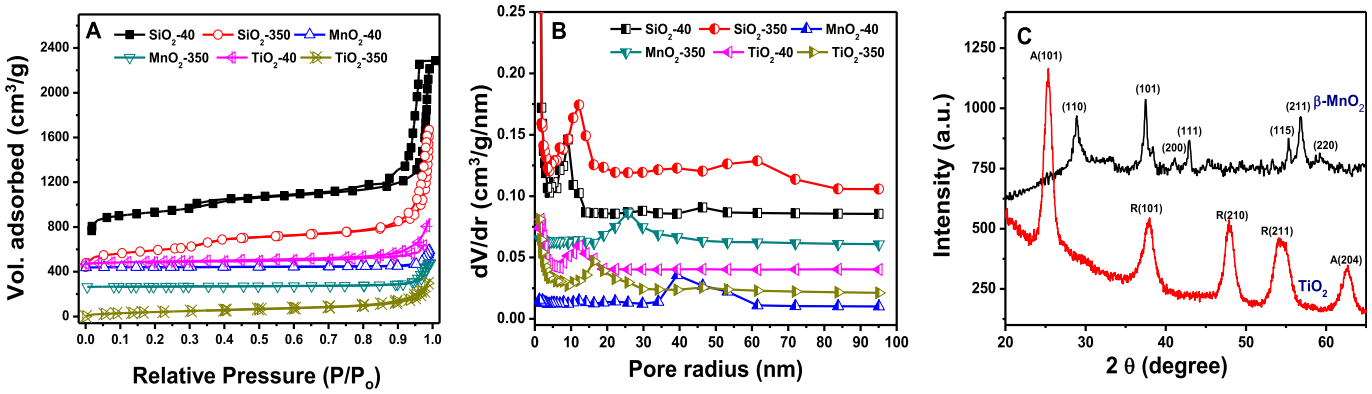

Fig. 1. A) Nitrogen adsorption-desorption isotherm, B) pore size distribution (by BJH method) plots for the monoliths and C) XRD pattern of metal-oxide monoliths.

Table 1
Textural characteristics for the silica and metal-oxide monoliths determined from nitrogen sorption measurements.

Sample Name	MW of PEG (g mol^{-1})	BET area (m^2 g^{-1})	Pore diameter (nm)	Pore volume (cm^3 g^{-1})
SiO_2-40	4000	691	13.2	2.3
SiO_2-350	35,000	761	18.4	1.4
MnO_2-40	4000	19	47.7	0.2
MnO_2-350	35,000	27	25	0.1
TiO_2-40	4000	140	18	0.6
TiO_2-350	35,000	220	9.4	0.5

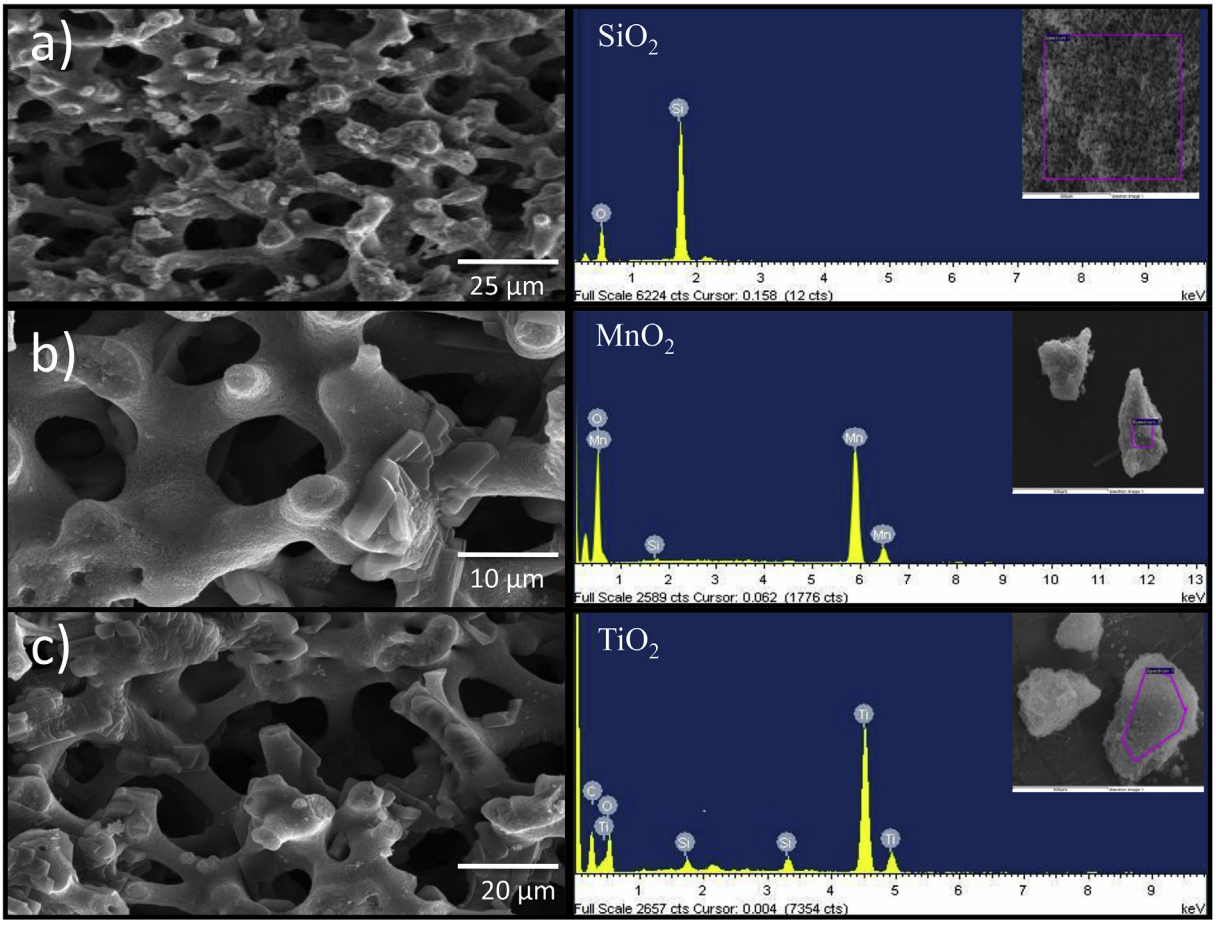

Fig. 2. FESEM images and corresponding energy-dispersive spectrum of A) SiO_2 – 350 B) MnO_2- 350 and C) TiO_2- 350 monoliths.

3.1. Adsorption studies

3.1.1. Effect of pH

Adsorption of Pb(II) & Cd(II) in the pores of monoliths depends on the pH of the solution, because of the degree of ionization, surface binding sites of adsorbents and the chemistry of adsorbates. Adsorption of Pb(II) & Cd(II) by silica and metal oxide monoliths were studied at a pH range from 3 to 10. pH values were adjusted by addition of either NaOH or HNO_3 in the synthetic solution of Pb(II) & Cd(II) [36–38]. Fig. 3 (A & B) shows plots for the effect of pH on Pb(II) & Cd(II) adsorption efficiency of metal-oxide monoliths. Maximum metal ion removal was observed at pH 6 for all the monoliths. Under the acidic conditions (at low pH), the surface of the adsorbents was surrounded by H^+ ions that compete with metal ions, which prevented the metal ions from approaching the binding sites on the adsorbent. Whereas at high pH values, metal ions were adsorbed due to the negatively charged ions. With the increase of pH, metal-oxides form deprotonated oxides and results in an increase in adsorption of metal ions on the surface of metal oxides due to which electrostatic repulsion force between surface and metal ions decreases.

3.1.2. Effect of contact time

The effect of contact time was analyzed between 15 and 80 min for the adsorption of metal ions by monoliths (Fig. 3C and D). The initial concentration of metal salts was kept 100 mg/L at pH 6. The equilibrium time depends on upon the initial concentration of Pb(II) & Cd(II) ions in the solution. Pb(II) & Cd(II) ions were quantitatively absorbed by the metal oxide monoliths from the synthetic solution even after a short time of exposure (<15 min). Since there was no significant increase in metal ions sorption after 65 min, the reaction time of 80 min was kept for auxiliary experiments [39–43].

3.1.3. Effect of metal ions concentration

Effect of the metal ions concentration on the monolith (0.02 g) dependent adsorption process was studied by changing the initial Pb(II) & Cd(II) concentrations in the range of 10–50 mg/L at most effective pH (6) and at room temperature (Fig. SI 2). The adsorption of metal-ions at different concentrations was fast during the early stage, which slowly decreases with further adsorption process until equilibrium was reached. Fast adsorption at small time was due to the large availability of adsorption sites on the surface of metal-oxides. The results confirmed that the removal efficiency of metal ions was directly proportional to the initial concentration of the metal ions [44–47]. The removal percentage of Pb(II) & Cd(II) by SiO_2, MnO_2, and TiO_2 monoliths were found to be 88–94%, 94–96% and 92–98% respectively of different metal ion concentration (Fig. SI 2).

3.2. Adsorption kinetics

The kinetics of Pb(II) & Cd(II) adsorption on metal oxides were also evaluated using Lagergren's first order rate equation and pseudo-second-order kinetic model [48–50]. The Lagergren's first-order rate equation is usually used to predict adsorption kinetics

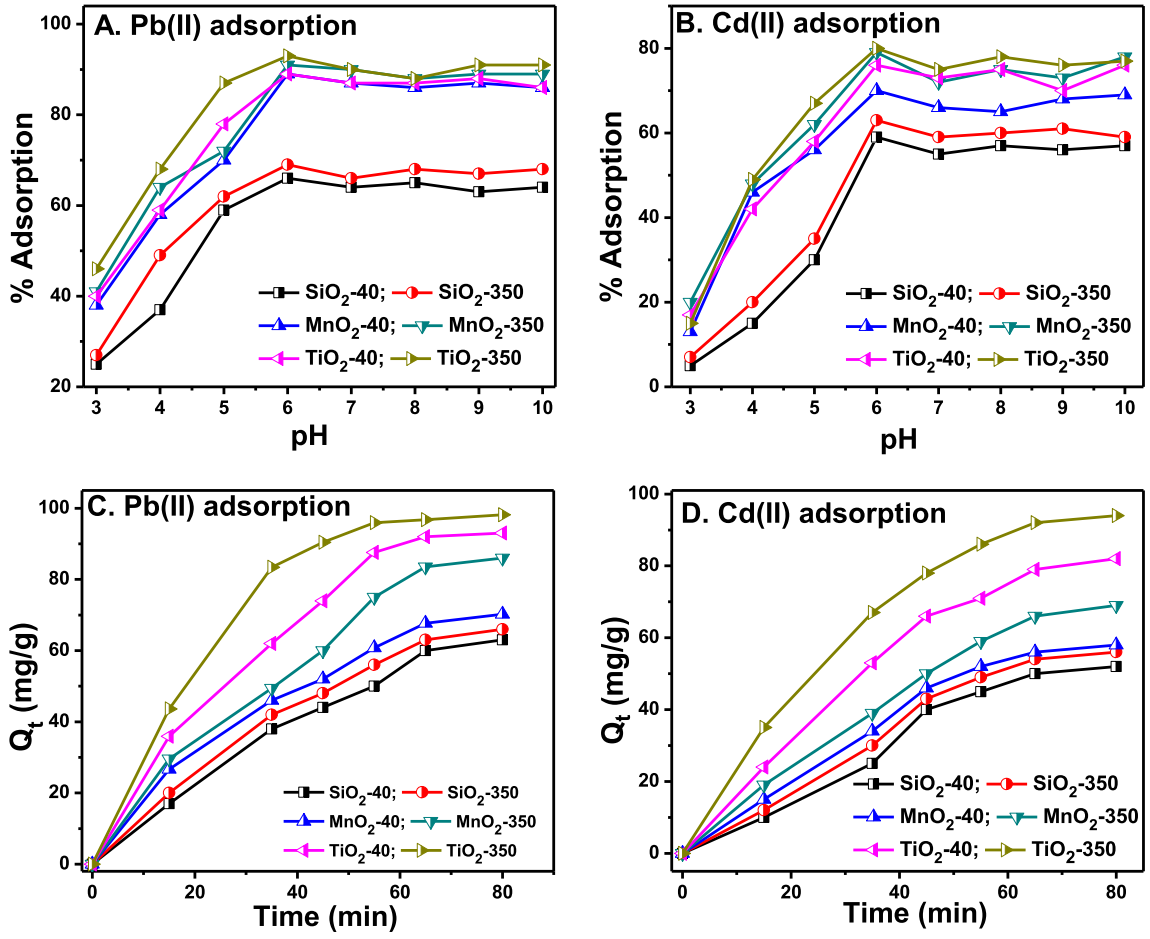

Fig. 3. Adsorption capacity of silica and metal oxide monoliths to show effect of pH on the metal ions A) & B) and effect of time on with initial concentration (100 mg/L) C) & D).

and is expressed as;

$$\log(q_e - q_t) = \log(q_e) - \frac{K_1}{2.303}t \quad (2)$$

The pseudo-second-order rate equation is expressed as;

$$\frac{t}{q_t} = \frac{1}{k_2 q_e^2} + \frac{t}{q_e} \quad (3)$$

where q_e and q_t are the amount of metal ions (mg/g) adsorbed at equilibrium and at any given time t (min) respectively. While K_1 is the rate constant for the pseudo-first order reaction for adsorption (min^{-1}) and K_2 is the rate constant for pseudo-second order reaction (g/mg min) [51]. Linear fit plots of pseudo-first order and pseudo-second order for SiO_2, MnO_2 and TiO_2 monoliths on the adsorption of Pb(II) & Cd(II) ions are shown in Fig. SI 3 and SI 4, respectively. The pseudo-second order kinetic model coordinates well with the adsorption of metal-ions, which suggested that the metal-ions adsorption process might be mostly controlled by chemisorption.

3.3. Adsorption isotherms

Adsorption isotherm gives proper quantitation of effectiveness of adsorption. The relationship between the concentration of adsorbed and dissolved adsorbate at equilibrium along with the interactive behavior between the adsorbate and adsorbent can also describe by adsorption isotherm. In this study, Langmuir and Freundlich isotherm models were used to analyze the adsorption mechanisms, through which experimental results of metal ions can be explained in a wide range of concentrations [52]. The Langmuir equation is expressed as follows;

$$\frac{C_e}{q_e} = \frac{1}{Q_o b} + \frac{C_e}{Q_o} \quad (4)$$

where the adsorption capacity at equilibrium is q_e (mg/g) and the maximum amount of the Pb(II) & Cd(II) adsorbed per unit weight of the adsorbent is Q_0 (mg/g).

When the surface is entirely covered with metal ions, Q_0 represents the adsorption capacity, helping in the assessment of adsorption act of different adsorbents. Langmuir equilibrium constant (b) which is interrelated to the similarity of the connecting spots, shows the bond energy for the adsorption reaction. The linear plots of C_e/q_e vs. C_e propose the validity of the Langmuir isotherms and the values of Q_0 and b are obtained from slope and intercepts of the plots [53–55]. Plots for Langmuir isotherm for adsorption on silica and metal-oxide monoliths for Pb(II) & Cd(II) are shown in Fig. 4.

The Freundlich isotherm is a resultant model of multilayer adsorption on the adsorbent. It can be described as:

$$\log q_e = \log K_f + \frac{\log C_e}{n} \quad (5)$$

Freundlich constants, K_f ($mg^{1-1/n}L^{1/n}\ g^{-1}$) and n, depict the adsorption capacity and intensity, respectively [56,57]. Freundlich isotherm plot for Pb(II) and Cd(II) adsorption on SiO_2, MnO_2 and TiO_2 are shown in Fig. 5. Although, SiO_2 monolith has high surface area resulted in a decrease in maximum adsorption. As, adsorption mechanism is generally based on an ion exchange or formation of bidentate binuclear surface complexes between metal oxides and metal ions [58,59], so metal oxides are more competent to hold other metal ions. In both cases (MnO_2 and TiO_2 monoliths), the bond between heavy metal ions and metal oxide surface is strong due to which metal oxides can adsorb metal ions from very diluted

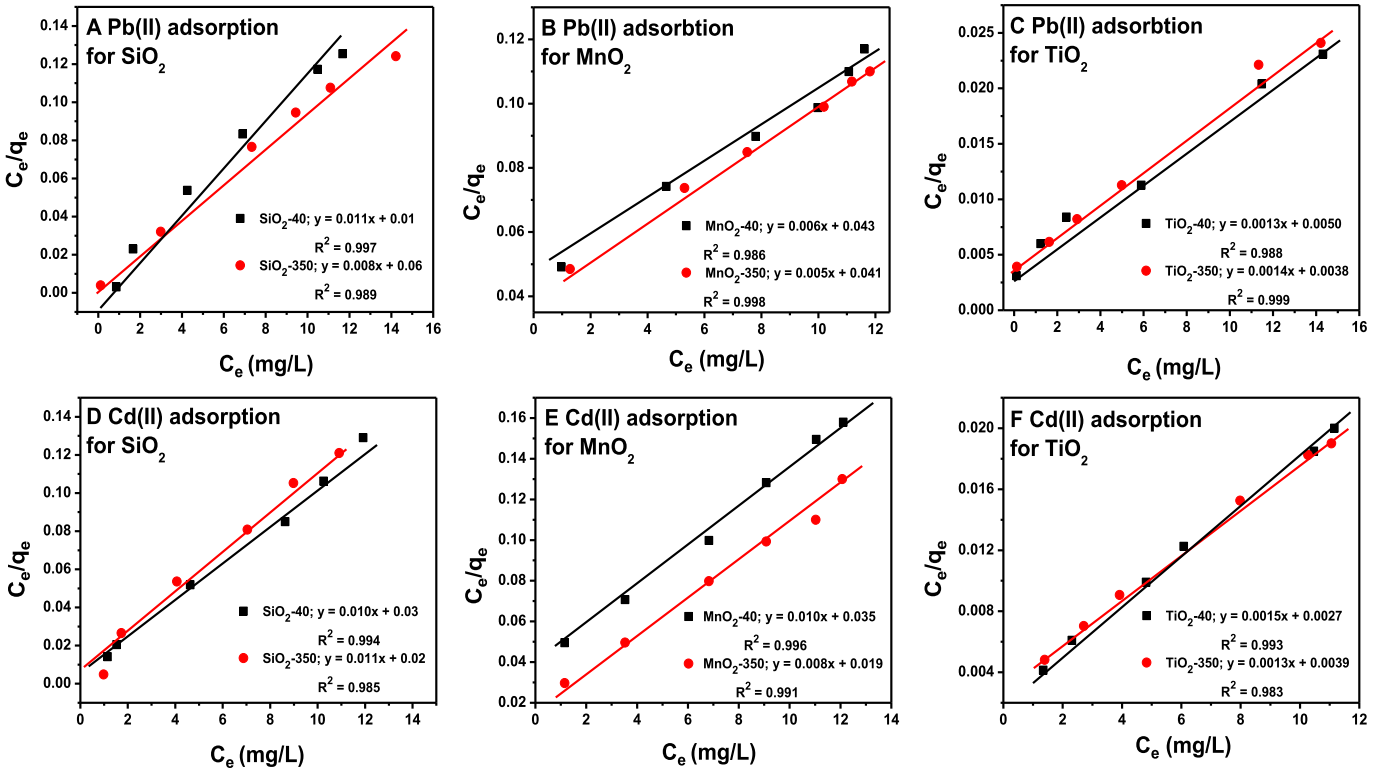

Fig. 4. Langmuir isotherm plot for Pb(II) and Cd(II) adsorption on SiO_2 and metal oxide monoliths.

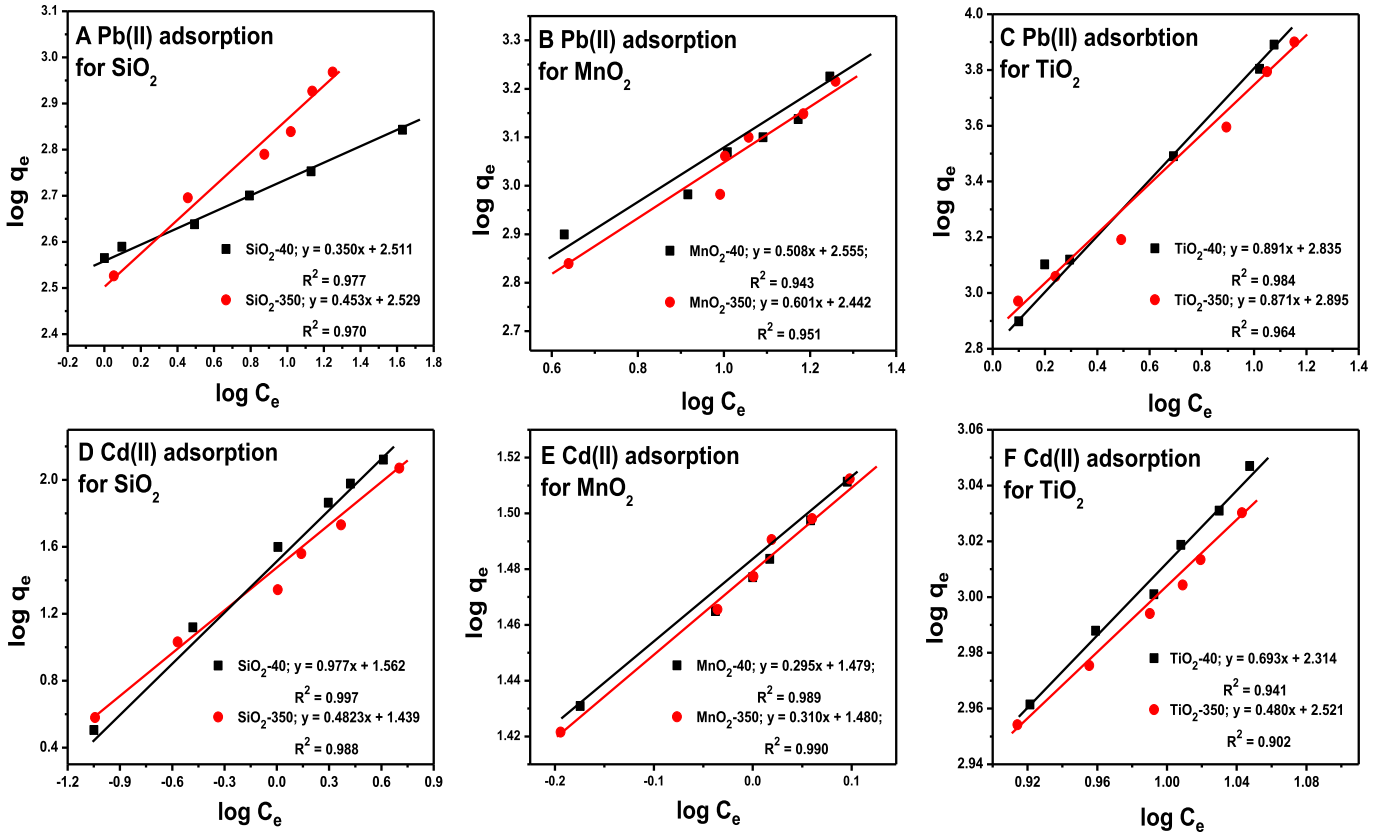

Fig. 5. Freundlich isotherm plot for Pb(II) and Cd(II) adsorption on SiO_2 and metal oxide monoliths.

metal ion solutions. Therefore; in spite of having a lesser surface area, MnO_2 monoliths (in compared to SiO_2 monoliths) has maximum adsorption value almost as high as SiO_2 monoliths. The maximum adsorption capacities for Pb(II) & Cd(II) were described in Table 2. Monolayer adsorption capacity calculated from the Langmuir model indicates the better applicability due to higher values of correlation coefficients (R^2). Table 3 shows a comparison study of maximum sorption capacities of metal ions reported in the literature. Therefore, it could be conceived that the as synthesized metal oxide monoliths could be employed as an alternative adsorbent for Pb(II) & Cd(II) adsorption at low concentrations.

3.4. Effect of temperature on adsorption

To determine the effect of temperature on the surface of hierarchically porous metal oxides for Pb(II) & Cd(II) adsorption, adsorption experiments was monitored at various temperatures (303, 313 and 323 K). Increase in temperature results in a decrease of the values of $\ln(q_e/C_e)$ and also 1000/T which specifies the exothermic nature of the adsorption process [69,70]. At different temperatures the values of $\ln(q_e/C_e)$ are treated according to Van't Hoff equation;

$$\ln\left(\frac{q_e}{C_e}\right) = \frac{-\Delta H}{RT} + \frac{\Delta S}{R} \quad (6)$$

where R is the universal gas constant (8.314 $Jmol^{-1}K^{-1}$) and T is the absolute temperature. The slope (ΔH/R) and intercept (ΔS/R) were evaluated from the plot between $\ln(q_e/C_e)$ and 1/T as shown in Fig. SI 5. At higher temperature, the adsorption process was also increased as Pb(II) and Cd(II) were adsorbed on the surface of mesoporous metal oxides. Gibbs free energy (ΔG) for adsorption of metal ions was calculated as of the following relation; [70,71]

$$\Delta G = \Delta H - T\Delta S \quad (7)$$

Table SI 6 shows the negative values of ΔG which confirms the spontaneity of the adsorption reactions.

3.5. Reusability

As stated in above, a strong bond formed between metal-oxides and metal-ions at the time of adsorption, which is essential for

Table 2
Langmuir and Freundlich constants and correlation coefficients for adsorption of Pb(II) & Cd(II) on metal-oxide monoliths.

Sample Name	Metal ions	Langmuir			Freundlich		
		Q_0[a]	b	R^2	K_f[b]	n	R^2
SiO_2-40	Pb(II)	90.9	1.1	0.997	383.7	6.02	0.983
	Cd(II)	100	0.3	0.998	36.47	1.02	0.997
SiO_2-350	Pb(II)	125	0.1	0.996	338.06	2.20	0.970
	Cd(II)	90.9	0.5	0.999	27.4	1.21	0.988
MnO_2-40	Pb(II)	166.6	0.13	0.995	358.9	1.96	0.943
	Cd(II)	100	0.28	0.999	30.13	3.38	0.989
MnO_2-350	Pb(II)	200	0.12	0.995	276.69	1.66	0.951
	Cd(II)	125	0.42	0.984	30.19	3.22	0.990
TiO_2-40	Pb(II)	769.2	0.245	0.988	683.9	1.12	0.984
	Cd(II)	667	0.555	0.993	206.06	1.44	0.941
TiO_2-350	Pb(II)	857	0.307	0.999	785.23	1.14	0.964
	Cd(II)	770	0.333	0.983	331.8	2.08	0.902

[a] (mg g^{-1}).
[b] ($mg^{1-1/n}L^{1/n}$ g^{-1}).

Table 3
A comparative account of the adsorption efficiency of heavy metal-ions by different metal-oxide nanostructures.

Adsorbents	Surface area (m^2/g)	Metal-ions	Maximum adsorption		Conditions	References
			(mg/g)	%		
TiO_2 nanoparticles	–	Pb(II)	–	44.7	Time- 60–90 min	[60]
		Cd(II)		25		
Nano- TiO_2	–	Pb(II)	–	100	pH-2	[61]
$MnFe_2O_4$- G composite	79.30	Pb(II)	100	–	pH- 2-8	[62]
		Cd(II)	76.9		Time-220 min	
GO-TiO_2	–	Pb(II)	65.6	–	pH- 5.6	[63]
		Cd(II)	72.8		Time- 12 h	
Silica nanotubes (SNT)	–	Pb(II)	42.85	–	pH-4, 7, 9, Temp-30 °C	[64]
					Time-240 min	
ß-MnO_2	83.5	Cd(II)	12.9	–	Temp-20-50 °C	[65]
					pH-4-6	
Mesoporous silica	198.3	Cu(II)	36.38	–	pH-2-7	[66]
Silica monoliths	565	Cu(II)	145.98	–	pH-7	[67]
SiO_2 monolith	761	Pb(II)	125	–	pH-6	Present study
MnO_2 monolith	27	Cd(II)	90.9		Temp-30 °C	
TiO_2 monolith	220	Pb(II)	200		Time-80 min	
		Cd(II)	125			
		Pb(II)	857			
		Cd(II)	770			

complete removal of metal-ions from water. In this case, no specific filtration techniques are required for metal-oxide extraction due to its large size. Also the metal oxide monoliths possess a robust and strong mechanical structure that can sustain water flow for extended periods of time, which will increase the adsorption capacity. The micrometer-sized overall structure with mesoporosity of monoliths provides the necessary mechanical robustness against wear and tear; while their nanostructure provides the high surface area as well as the high removal capacity for heavy metal ions. Though, regeneration or reusability of metal oxide bear great challenges, still by treating the saturated metal-oxides by 2M NaOH for 5 h, moderately regenerated metal-oxides can be obtained [72]. Here, we have checked the reusability of synthesized monoliths for 3 cycles and observed that, the removal efficiency decreases upto 35–40% (Fig. SI 7).

4. Conclusion

Two different high surface area SiO_2 monoliths were turning out to porous MnO_2 and TiO_2 monoliths via nanocasting method. Hierarchically porous metal oxide monoliths exhibited excellent adsorption performance for Pb(II) & Cd(II). The adsorption studies were conducted in different batches. The removal percentage of Pb(II) & Cd(II) by SiO_2, MnO_2, and TiO_2 monoliths were observed 88–94%, 94–96% and 92–98%, respectively. Thermodynamic studies on the surface of hierarchically porous metal oxides for Pb(II) & Cd(II) adsorption were monitored at various temperatures (303, 313 and 323 K). Negative ΔG value suggests that the adsorption process was spontaneous. Synthesized monoliths are in the cm range scale (0.5 cm in diameter and 0.8 cm in length) which gave a unique advantage in the form of efficient and low-cost recovery over existing systems. Porous monoliths with large structure are highly efficient for heavy metal ions removal and results were found to be comparable or better than other metal oxide nanocomposites in literature. These advantages will make the nanocasted metal oxide monolithic system a potential candidate for development of a user-friendly, low-cost device for the treatment of large polluted water bodies.

Acknowledgement

The authors are thankful to BRNS (Grant no: 34/14/63/2014) for fellowship and other financial assistance. We are also thankful to DST (Grant no: SB/FT/CS-178/2013), DST-FIST, Sprint Testing solutions-Mumbai and Thapar University for providing instrumental facilities.

Appendix A. Supplementary data

Supplementary data related to this article can be found at http://dx.doi.org/10.1016/j.jallcom.2017.05.260.

References

[1] J.-P. Zou, H.-L. Liu, J. Luo, Q.-J. Xing, H.-M. Du, X.-H. Jiang, X.-B. Luo, S.-L. Luo, S.L. Suib, Three-Dimensional reduced graphene oxide coupled with Mn_3O_4 for highly efficient removal of Sb(III) and Sb(V) from water, ACS Appl. Mater. Interfaces 8 (2016) 8140–18149.
[2] S. Khan, C. Chao, M. Waqas, H.P.H. Arp, Y.G. Zhu, Sewage sludgebiochar influence upon rice (Oryza sativa L) yield, metal bioaccumulation and greenhouse gas emissions from acidic paddy soil, Environ. Sci. Technol. 47 (2013) 8624–8632.
[3] S.J.S. Flora, G.J.S. Flora, G. Saxena, Environmental occurrence, health effects and management of lead poisoning, in: S.B. Cascas, J. Sordo (Eds.), Lead: Chemistry, Analytical Aspects, Environmental Impacts and Health Effects, Elsevier, Netherlands, 2006, pp. 158–228.
[4] A. Mittal, J. Mittal, A. Malviya, V.K. Gupta, Adsorptive removal of hazardous anionic dye "Congo red" from wastewater using waste materials and recovery by desorption, J. Colloid Interf. Sci. 340 (2009) 16–26.
[5] Z.L. He, X.E. Yang, P.J. Stoffella, Trace elements in agro ecosystems and impacts on the environment, J. Trace Elem. Med. Biol. 19 (2005) 125–140.
[6] H. Bradl, Heavy Metals in the Environment: Origin, Interaction and Remediation, vol. 6, Academic, London, 2002.
[7] C.K. Ahn, D. Parka, S.H. Woob, J.M. Parka, Removal of cationic heavy metal from aqueous solution by activated carbon impregnated with anionic surfactants, J. Hazard. Mater 164 (2009) 1130–1136.
[8] M. Alavi, A. Morsali, Syntheses and characterization of $Mg(OH)_2$ and MgO nanostructures by ultrasonic method, Ultrason. Sonochem. 17 (2010) 441–446.
[9] S. Mahdavi, M. Jalali, A. Afkhami, Heavy metals removal from aqueous solutions using TiO_2, MgO, and Al_2O_3 nanoparticles, Chem. Eng. Comm. 200 (2013) 448–470.
[10] S. Debnath, U.C. Ghosh, Equilibrium modeling of single and binary adsorption of Cd(II) and Cu(II) onto agglomerated nano structured titanium(IV) oxide, Desalination 273 (2011) 330–342.
[11] W. Si, Y. Wang, S. Zhao, F. Hu, J. Li, A facile method for in situ preparation of the MnO_2/$LaMnO_3$ catalyst for the removal of toluene, Environ. Sci. Technol. 50 (2016) 4572–4578.
[12] A. Mehta, A. Mishra, M. Sharma, S. Singh, S. Basu, Effect of silica/titania ratio on enhanced photooxidation of industrial hazardous materials by microwave treated mesoporous SBA-15/TiO_2 nanocomposites, J. Nanopart. Res. 18 (2016) 1–9.
[13] L. Zhang, J. Lian, L. Wu, Z. Duan, J. Jiang, L. Zhao, Synthesis of a thin-layer MnO_2 nanosheet-coated Fe_3O_4 nanocomposite as a magnetically separable photocatalyst, Langmuir 30 (2014) 7006–7013.
[14] J.-S. Hu, L.-S. Zhong, W.-G. Song, L.-J. Wan, Synthesis of hierarchically

structured metal oxides and their application in heavy metal ion removal, Adv. Mater 20 (2008) 2977–2982.
[15] T.A. Saleh, V.K. Gupta, Column with CNT/magnesium oxide composite for lead(II) removal from water, Environ. Sci. Pollut. Res. 19 (2012) 1224–1228.
[16] M.I. Zaman, S. Mustafa, S. Khan, B. Xing, Effect of phosphate complexation on Cd^{2+} sorption by manganese dioxide (β- MnO_2), J. Colloid Interf. Sci. 330 (2009) 9–19.
[17] L. Dong, Z. Zhu, H. Ma, Y. Qiu, J. Zhao, Simultaneous adsorption of lead and cadmium on MnO2-loaded resin, J. Environ. Sci. 22 (2010) 225–229.
[18] Y.-C. Lee, J.W. Yang, Self-assembled flower-like TiO_2 on exfoliated graphite oxide for heavy metal removal, J. Ind. Eng. Chem. 18 (2012) 1178–1185.
[19] N. Wu, H. Wei, L. Zhang, Efficient removal of heavy metal ions with biopolymer template synthesized mesoporous titania beads of hundreds of micrometers size, Environ. Sci. Technol. 46 (2012) 419–425.
[20] J. Hu, H.J. Shipley, Regeneration of spent TiO_2 nanoparticles for Pb (II), Cu (II), and Zn (II) removal, Environ. Sci. Pollut. Res. 20 (2013) 5125–5137.
[21] J.-H. Smått, C. Weidenthaler, J.B. Rosenholm, M. Linden, Hierarchically porous metal oxide monoliths prepared by the nanocasting route, Chem. Mater 18 (2006) 1443–1450.
[22] A.-H. Lu, J.-H. Smatt, M. Linden, Combined surface and volume templating of highly porous nanocast carbon monoliths, Adv. Funct. Mater 15 (2005) 865–871.
[23] A.-H. Lu, J.-H. Smatt, S. Backlund, M. Linden, Easy and flexible preparation of nanocasted carbon monoliths exhibiting a multimodal hierarchical porosity, Micropor. Mesopor. Mater 72 (2004) 59–65.
[24] B. Tian, X. Liu, H. Yang, S. Xie, C. Yu, B. Tu, D. Zhao, General synthesis of ordered crystallized metal oxide nanoarrays replicated by microwave digested mesoporous silica, Adv. Mater 15 (2003) 1370–1374.
[25] G. Hasegawa, K. Kanamori, T. Kiyomura, H. Kurata, T. Abe, K. Nakanishi, Hierarchically porous carbon monoliths comprising ordered mesoporous nanorod assemblies for high-voltage aqueous supercapacitors, Chem. Mater 28 (2016) 3944–3950.
[26] K. Zhu, B. Yue, W. Zhou, H. He, Preparation of three-dimensional chromium oxide porous single crystals templated by SBA-15, Chem. Comm. 1 (2003) 98–99.
[27] H. Yang, Q. Shi, B. Tian, Q. Lu, F. Gao, S. Xie, J. Fan, C. Yu, B. Tu, D. Zhao, One-step nanocasting synthesis of highly ordered single crystalline indium oxide nanowire arrays from mesostructured frameworks, J. Am. Chem. Soc. 125 (2003) 4724–4725.
[28] S.C. Laha, R. Ryoo, Synthesis of thermally stable mesoporous cerium oxide with nanocrystalline frameworks using mesoporous silica templates, Chem. Comm. 17 (2003) 2138–2139.
[29] J.-H. Smatt, F.M. Sayler, A.J. Grano, M.G. Bakker, formation of hierarchically porous metal oxide and metal monoliths by nanocasting into silica monoliths, Adv. Eng. Mater 14 (2012) 1059–1073.
[30] W. Cheng, F. Rechberger, M. Niederberger, Three-Dimensional assembly of yttrium oxide nanosheets into luminescent aerogel monoliths with outstanding adsorption properties, ACS Nano 10 (2016) 2467–2475.
[31] T. Sano, Y. Oumi, Mesoporous silica as nanoreactor for olefin polymerization, Catal. Surv. Asia 8 (2004) 295–304.
[32] Y. Sato, K. Nakanishi, K. Hirao, H. Jinnai, M. Shibayama, Y.B. Melnichenko, G.D. Wignall, Formation of ordered macropores and templated nanopores in silica sol–gel system incorporated with EO–PO–EO triblock copolymer, Colloids Surf. A. Physicochem. Eng. Asp. 187–188 (2001) 117–122.
[33] K. Nakanishi, Supramolecular templating of mesopores in phase-separating silica sol-gels incorporated with cationic surfactant, J. Sol-Gel Sci. Tech. 26 (2003) 567–570.
[34] S. Jana, S. Basu, S. Pande, S.K. Ghosh, T. Pal, Shape-selective synthesis, magnetic properties, and catalytic activity of single crystalline β-MnO2 nanoparticles, J. Phys. Chem. C 111 (2007) 16272–16277.
[35] Z. Xu, C. Huang, L. Wang, X. Pan, L. Qin, X. Guo, G. Zhang, Functionalized Fe_2O_3 nanoparticles on TiO_2 nanotube as efficient visible light-active photo-fenton catalyst, Ind. Eng. Chem. Res. 54 (2015) 4593–4602.
[36] A. Jumasiah, T.G. Chuah, J. Gimbon, T.S.Y. Choong, I. Azni, Adsorption of basic dye onto palm kernel shell activated carbon: sorption equilibrium and kinetics studies, Desalination 186 (2005) 57–64.
[37] N.K. Amin, Removal of reactive dye from aqueous solutions by adsorption onto activated carbons prepared from sugarcane bagasse pith, Desalination 223 (2008) 152–161.
[38] A. Mittal, D. Kaur, J. Mittal, Batch and bulk removal of a triarylmethane dye, Fast Green FCF, from wastewater by adsorption over waste materials, J. Hazard. Mater 163 (2009) 568–577.
[39] C.A. Basar, Applicability of the various adsorption models of three dyes adsorption onto activated carbon prepared waste apricot, J. Hazard. Mater B135 (2006) 232–241.
[40] P.K. Malik, Use of activated carbons prepared from sawdust and rice-husk for adsorption of acid dyes: a case study of acid yellow 36, Dyes Pigm 56 (2003) 239–249.
[41] S. Chatterjee, S. Chatterjee, B.P. Chatterjee, A.K. Guha, Adsorptive removal of Congo red, a carcinogenic textile dye by chitosan hydrobeads: binding mechanism, equilibrium and kinetics, Colloids Surf. A 299 (2007) 146–152.
[42] S. Rengaraj, Y. Kim, C.K. Joo, J. Yi, Removal of copper from aqueous solutions by aminated and protonated mesoporous aluminas: kinetics and equilibrium, J. Colloid Interface Sci. 273 (2004) 14–21.
[43] F. Colak, N. Atar, A. Olgun, Biosorption, of acidic dyes from aqueous solution by Paenibacillus macerans: kinetic, thermodynamic and equilibrium studies, Chem. Eng. J. 150 (2009) 122–130.
[44] A. Shukla, Y. Zhang, P. Dubey, J.L. Margrave, S.S. Shukla, The role of sawdust in the removal of unwanted materials from water, J. Hazard. Mater B95 (2002) 137–152.
[45] G. Donmez, Z. Aksu, Removal of chromium (VI) from saline wastewaters by Dunaliella species, Process Biochem. 38 (2002) 751–762.
[46] N. Kannan, M.M. Susndaram, Kinetics and mechanism of removal of methylene blue by adsorption on various carbons-a comparative study, Dyes Pigm. 51 (2001) 25–40.
[47] I.D. Mall, V.C. Srivastava, N.K. Agarwal, I.M. Mishra, Removal of Congo red from aqueous solution by bagasse fly ash and activated carbon: kinetic study and equilibrium isotherm analyses, Chemosphere 61 (2005) 492–501.
[48] W.J. Thomson, Introduction to Transport Phenomena, Prentice Hall PTR, Upper Saddle River, NJ, 2000.
[49] C. Lu, Y.-L. Chung, K.-F. Chang, Adsorption thermodynamic and kinetic studies of trihalomethanes on multiwalled carbon nanotubes, J. Hazard. Mater B138 (2006) 304–310.
[50] A. Mittal, D. Kaur, J. Mittal, Applicability of waste materials— bottom ash and deoiled soya—as adsorbents for the removal and recovery of a hazardous dye, brilliant green, J. Colloid Interface Sci. 326 (2008) 8–17.
[51] M.J. Iqbal, M.N. Ashiq, Adsorption of dyes from aqueous solutions on activated charcoal, J. Hazard. Mater B139 (2007) 57–66.
[52] M. Xu, Y.S. Zhang, Z.M. Zhang, Y. Shen, Study on the adsorption of Ca^{2+}, Cd^{2+} and Pb^{2+} by magnetic Fe_3O_4 yeast treated with EDTA dianhydride, Chem. Eng. J. 168 (2011) 737–745.
[53] I. Langmuir, The constitution and fundamental properties of solids and liquids, J. Am. Chem. Soc. 38 (1916) 2221–2295.
[54] O. Abdelwahab, Evaluation of the use of loofa activated carbons as potential adsorbents for aqueous solutions containing dye, Desalination 222 (2008) 357–367.
[55] A.H. Chen, C.Y. Yang, C.Y. Chen, C.Y. Chen, C.W. Chen, The chemically cross-linked metal-complexed chitosans for comparative adsorptions of Cu(II), Zn(II), Ni(II) and Pb(II) ions in aqueous medium, J. Hazard. Mater 163 (2009) 1068–1075.
[56] P. Waranusantigul, P. Pokethitiyook, M. Kruatrachue, E.S. Upatham, Kinetics of basic dye (methylene blue) biosorption by giant duckweed (Spirrodella polyrrhiza), Environ. Pollut. 125 (2003) 385–392.
[57] X.L. Tan, X.K. Wang, M. Fang, C.L. Chen, Sorption and desorption of Th(IV) on nanoparticles of anatase studied by batch and spectroscopy methods, Colloid. Surf. A 296 (2007) 109–116.
[58] J.-S. Hu, L.-S. Zhong, W.-G. Song, L.-J. Wan, Synthesis of hierarchically structured metal oxides and their application in heavy metal ion removal, Adv. Mater. 20 (2008) 2977–2982.
[59] X.J. Peng, Z.K. Luan, J. Ding, Z.H. Di, Y.H. Li, B.H. Tian, Ceria nanoparticles supported on carbon nanotubes for the removal of arsenate from water, Mater. Lett. 59 (2005) 399.
[60] S. Mahdavi, M. Jalali, A. Afkhami, Heavy metals removal from aqueous solutions using TiO_2, MgO, and Al_2O_3 nanoparticles, Chem. Eng. Commun. 200 (2013) 448–470.
[61] J. Hu, H.J. Shipley, Shipley Regeneration of spent TiO_2 nanoparticles for Pb (II), Cu (II), and Zn (II) removal, Environ. Sci. Pollut. Res. 20 (2013) 5125–5137.
[62] S. Chella, P. Kollu, E.V.P.R. Komarala, S. Doshi, M. Saranya, S. Felix, R. Ramachandran, P. Saravanan, V.L. Koneru, V. Venugopal, S.K. Jeong, A.N. Grace, Solvothermal synthesis of $MnFe_2O_4$-graphene composite—investigation of its adsorption and antimicrobial properties, Appl. Surf. Sci. 327 (2015) 27–36.
[63] Y.-C. Lee, J.-W. Yang, Self-assembled flower-like TiO_2 on exfoliated graphite oxide for heavy metal removal, J. Indus. Eng. Chem. 18 (2012) 1178–1185.
[64] P. Wang, M. Du, H. Zhu, S. Bao, T. Yang, M. Zou, Structure regulation of silica nanotubes and their adsorption behaviors for heavy metal ions: pH effect, kinetics, isotherms and mechanism, J. Hazard. Mater 286 (2015) 533–544.
[65] Md I. Zaman, S. Mustafa, S. Khan, B. Xing, Effect of phosphate complexation on Cd^{2+} sorption by manganese dioxide (ß-MnO_2), J. Colloid Interf. Sci. 330 (2009) 9–19.
[66] X. Xue, F. Li, Removal of Cu(II) from aqueous solution by adsorption onto functionalized SBA-16 mesoporous silica, Micropor. Mesopor. Mater 116 (2008) 116–122.
[67] Md R. Awual, T. Yaita, S.A. El-Safty, H. Shiwaku, S. Suzuki, Y. Okamoto, Copper (II) ions capturing from water using ligand modified a new type mesoporous adsorbent, Chem. Eng. J. 221 (2013) 322–330.
[69] T.-T. Li, Y.-G. Liu, Q.-Q. Peng, X.-J. Hu, T. Lia, H. Wang, M. Lu, Removal of lead (II) from aqueous solution with ethylenediamine-modified yeast biomass coated with magnetic chitosan microparticles: kinetic and equilibrium modeling, Chem. Eng. J. 214 (2013) 189–197.
[70] G.C. Panda, S.K. Das, A.K. Guha, Jute stick powder as a potential biomass for the removal of Congo red and rhodamine B from their aqueous solution, J. Hazard. Mater 164 (2009) 374–379.
[71] E. Eren, H. Gumus, A. Sarihan, Synthesis structural characterization and Pb(II) adsorption behavior of K- and H-birnessite samples, Desalination 279 (2011) 75–85.
[72] L.S. Zhong, J.S. Hu, A.M. Cao, Q. Liu, W.G. Song, L.J. Wan, 3D flowerlike ceria micro/nanocomposite structure and its application for water treatment and CO removal, Chem. Mater 19 (2007) 1648.